CHEMISTRY OF MATERIALS

ARTICLE

pubs.acs.org/cm

Ion-Exchange Synthesis, Crystal Structure, and Electrochemical Properties of $Li_2Ti_6O_{13}$

Kunimitsu Kataoka,*[,†,‡] Junji Awaka,[†] Norihito Kijima,[†] Hiroshi Hayakawa,[†] Ken-ichi Ohshima,[‡] and Junji Akimoto*[,†]

[†]National Institute of Advanced Industrial Science and Technology (AIST), 1-1-1 Higashi, Tsukuba, Ibaraki 305-8565, Japan

[‡]Graduate School of Pure and Applied Sciences, University of Tsukuba, 1-1-1 Tennodai, Tsukuba, Ibaraki 305-8573, Japan

Supporting Information

ABSTRACT: $Li_2Ti_6O_{13}$ was prepared from $Na_2Ti_6O_{13}$ as a parent compound via sodium/lithium ion exchange in molten $LiNO_3$ at 380 °C. It crystallizes in the monoclinic system, space group $C2/m$, and with the lattice parameters of a = 15.3065(4) Å, b = 3.74739(8) Å, c = 9.1404(2) Å, and β = 99.379(2)°. The crystal structure of $Li_2Ti_6O_{13}$ was refined to the conventional values of R_{wp} = 5.78% and R_p = 4.44% with a fit indicator of GOF = R_{wp}/R_e = 1.66 by Rietveld analysis using powder neutron diffraction data. The crystal structure of $Na_2Ti_6O_{13}$ was also reinvestigated using the single-crystal X-ray diffraction data with the final R value of 2.70%. The basic $(Ti_6O_{13})^{2-}$ framework in $Li_2Ti_6O_{13}$ was maintained nearly unchanged from that in the parent $Na_2Ti_6O_{13}$. The Li occupation site in the tunnel space shifted to y = 0.5 position from the original Na site in $Na_2Ti_6O_{13}$, and the moving resulted in the LiO_4 planar coordination in $Li_2Ti_6O_{13}$. The structural stability of $Li_2Ti_6O_{13}$ was confirmed by bond valence sums, the data of ^{7}Li-MAS NMR and high-temperature in situ XRD measurements, and the results of the present first-principles calculation by the FLAPW method. The electrochemical Li insertion/extraction experiments revealed the irreversible large Li insertion capacity of above 200 mAh g^{-1} at approximately 1.5 V for the first cycle and the stable reversible capacity of approximately 90−95 mAh g^{-1} during the following cycles. The total Li-ion conductivity in $Li_2Ti_6O_{13}$ was estimated to be $\sigma_{total} = 5.60 \times 10^{-6}$ S cm^{-1} at room temperature from the results of AC-impedance measurements. This value is comparable to that in the well-known good Li-ion conducting ramsdellite-type $Li_2Ti_3O_7$.

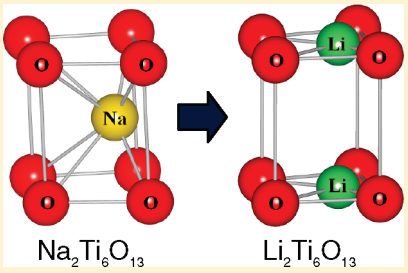

KEYWORDS: lithium titanate, $Li_2Ti_6O_{13}$, powder neutron diffraction, structure analysis, lithium ion conductor, lithium insertion, FLAPW calculation, ^{7}Li-MAS NMR, UV−vis, ion exchange

INTRODUCTION

Lithium titanium oxides in the Li_2O-TiO_2 system display a wide range of interesting chemical properties. Especially, the spinel-type $Li_4Ti_5O_{12}$ is attractive as one of the oxide negative electrode materials for advanced lithium-ion batteries,[1,2] because this compound exhibits the reversible Li insertion/extraction property at around 1.6 V (vs Li/Li^+). $Li_2Ti_3O_7$ with the ramsdellite-type tunnel structure is well-known to be a fast Li-ion conductor.[3] The reversible electrochemical Li-ion insertion/extraction reaction in this compound was also previously reported to occur at around 1.6 V (vs Li/Li^+), with a specific capacity of approximately 150 mAh g^{-1};[4−6] this value was attributed to the inserted Li content of 1.5 per $Li_2Ti_3O_7$ formula unit.

Another metastable form of $Li_2Ti_3O_7$ was prepared from $Na_2Ti_3O_7$ as a parent compound by ion exchange reaction in a molten $LiNO_3$.[7,8] The layered crystal structure of $Li_2Ti_3O_7$ was recently determined by Rietveld analysis using the powder X-ray diffraction data.[8] Although the basic framework in $Li_2Ti_3O_7$ remained nearly unchanged from that in the parent $Na_2Ti_3O_7$, the Li atoms in the interlayer space shifted from the original Na positions to the tetrahedral LiO_4 coordination sites in the layered $Li_2Ti_3O_7$ structure.[8] The reversible electrochemical Li insertion/extraction property was reported for the layered $Li_2Ti_3O_7$ around 1.3 V (vs Li/Li^+), with a specific capacity of about 150 mAh g^{-1},[8] the value of which was similar to that in the ramsdellite-type $Li_2Ti_3O_7$.

A similar sodium/lithium ion-exchange experiment was previously performed on $Na_2Ti_6O_{13}$ using molten $LiNO_3$ at 280 °C.[9] The crystal structure of $Na_2Ti_6O_{13}$ consists of zigzag chains of triple edge-shared TiO_6 octahedra with the rectangular tunnels where Na atoms are located.[10,11] It was previously reported that the lattice volume of the Li-ion exchanged product was strangely larger than that in the starting $Na_2Ti_6O_{13}$, suggesting the coordination change around alkali site after the sodium/lithium ion-exchange reaction.[9] Recently, the reversible electrochemical Li insertion/extraction reactions were reported in the nanosized $Na_2Ti_6O_{13}$[12] and the ion-exchanged $Li_2Ti_6O_{13}$.[13] However, the structural details of $Li_2Ti_6O_{13}$, especially the Li site positions, have not been revealed yet, to our knowledge. In addition, it was reported that the removal of Na was not complete in the

Received: December 28, 2010
Revised: March 22, 2011
Published: April 12, 2011

previous experimental condition.[9] Accordingly, chemical and structural properties of $Li_2Ti_6O_{13}$ should be precisely re-examined using the well-characterized samples. In addition, $Li_2Ti_6O_{13}$ is also interested in the one-dimensional Li-ion conduction property, as in the case of the ramsdellite-type $Li_2Ti_3O_7$.[3]

The present study has three main objectives. First, we prepared the $Li_2Ti_6O_{13}$ polycrystalline samples by sodium/lithium ion-exchange method using $Na_2Ti_6O_{13}$ as a parent compound, and we determined the precise crystal structure by powder neutron diffraction technique. The local structure around alkali atom in $Li_2Ti_6O_{13}$ was compared to that in the parernt $Na_2Ti_6O_{13}$. Second, the validity of the refined crystal structure was examined by ^{7}Li-MAS NMR measurement and first-principles calculation. Finally, we clarified the electrochemical properties of $Li_2Ti_6O_{13}$, in comparison with those of the parent $Na_2Ti_6O_{13}$.

EXPERIMENTAL SECTION

Sample Preparation. The precursor $Na_2Ti_6O_{13}$ was first prepared by a conventional solid-state reaction. A mixture of Na_2CO_3 (99.9% pure) and TiO_2 (99.99% pure) in a molar ratio of 1:6 was heated at 1073 K for 20 h in air. The resultant specimens were reground, and the same temperature program sequence was repeated once again. Small single crystals of $Na_2Ti_6O_{13}$ were also synthesized by heating the as-prepared $Na_2Ti_6O_{13}$ polycrystalline sample at 1723 K in a sealed Pt tube.

The polycrystalline $Li_2Ti_6O_{13}$ samples were prepared from $Na_2Ti_6O_{13}$ via ion-exchange at low temperatures. Sodium/lithium ion-exchange experiments were performed using the molten salt of $LiNO_3$ at various temperatures of 290, 320, 350, and 380 °C. After heat-treatment for 10 h in air, the reaction mixture was washed with water and ethanol, and then dried at 60 °C for 1 day in air.

Characterization. The phase purity and crystal structure of the obtained samples were characterized by powder X-ray diffraction (XRD) profiles measured at room temperature with Cu Kα radiation using a Rigaku RINT2550 V diffractometer (operating conditions: 40 kV, 200 mA) equipped with a curved graphite monochromator. The XRD intensity data were collected for 1 s at each 0.02° step over a 2θ range from 5° to 140° for the Rietveld refinement.

The chemical analysis of Li, Na, and Ti contents was performed by inductively coupled plasma-atomic emission spectroscopy (ICP-AES, Perkin-Elmer, Inc., Optima 3000). The particle morphology was verified by scanning electron microscopy (SEM) analysis (JEOL JSM-5400). The FTIR (Jasco, FT/IR-6100) spectrum was measured at room temperature by the KBr method. The selected area electron diffraction (SAED) pattern was observed using a transmission electron microscope (TEM, JEOL 2010) operating at 200 kV. The sample for the TEM observation was dispersed in ethanol by an ultrasonic bath, and a drop of this dispersion medium was added on microgrid.

To check for phase changes at high temperatures, the high temperature in situ XRD profiles were measured with Cu Kα radiation using a Panalytical X'part diffractometer (operating conditions: 45 kV, 40 mA) in 10 K steps over a temperature range from 303 to 1243 K. The XRD intensity data were collected for 1 s at each 0.033° step over a 2θ range from 10° to 80°.

The solid-state ^{7}Li magic-angle-spinning nuclear-magnetic-resonance (^{7}Li-MAS NMR) spectrum of the $Li_2Ti_6O_{13}$ sample was measured at room temperature at 116.676 MHz with a spinning rate 10 kHz for Li nuclei by saturation recovery method by a Chemagnetic CMX-300 spectrometer. The pulse width was 3.9 μs (π/2 pulse). The chemical shift was recorded relative to 1 M LiCl aqueous solution.

Optical absorption spectra (UV−vis) were measured using a Jasco V-550 spectrometer over the range 300−600 nm at room temperature. From the intersection values of the baseline and absorption band edge in the obtained spectra, we estimated the band gap energy of $Na_2Ti_6O_{13}$ and $Li_2Ti_6O_{13}$.

Crystal Structure Determination. Although the structure of the parent $Na_2Ti_6O_{13}$ was previously reported in the literature,[10,11] the atomic displacement parameters have not been clarified. In addition, the reported reliability value was relatively large (R = 15.1%).[11] Therefore, we first reinvestigated the crystal structure of $Na_2Ti_6O_{13}$ using the single-crystal X-ray diffraction data. A small needle-shaped $Na_2Ti_6O_{13}$ single crystal, 0.30 × 0.05 × 0.05 mm^3 in size, was used for the single-crystal X-ray diffraction experiment. Integrated intensity data were collected by single-crystal X-ray diffractometer with an imaging plate (Rigaku R-AXIS RAPID-II) using graphite-monochromatized Mo Kα radiation (operating condition: 50 kV, 40 mA) at 295 K. The structure refinement was carried out using a computer program Jana2006.[14]

The framework structure of $Li_2Ti_6O_{13}$ was first analyzed by ab initio structure determination method using the powder XRD data. The calculation was performed using the computer program N-TREOR[15] in EXPO2004,[16] Jana2006,[14] and Superflip.[17] The Rietveld refinement of $Li_2Ti_6O_{13}$ was performed by Jana2006 using powder neutron diffraction (ND) data measured at room temperature with wavelength λ = 1.8024 Å using a HERMES diffractometer (JAEA, JRR3M beamline T1−3).[18] The ND intensity data were collected in 0.05° steps over a 2θ range from 7° to 157°.

The nuclear scattering length density distribution (NSLDD) analysis was performed by the maximum entropy method (MEM) based on the Rietveld analysis using the powder ND data. The MEM calculation was carried out with the unit cell divided into 128 × 128 × 128 pixels using a MEM analysis program PRIMA.[19] The crystal structure and MEM images were drawn using the computer program VESTA.[20]

First-Principles Calculation. The electronic structures of $Na_2Ti_6O_{13}$ and $Li_2Ti_6O_{13}$ were calculated using the full-potential linearized augmented-plane-wave (FLAPW) method with the WIEN2k program.[21] The generalized gradient approximation (GGA) in the formulation of Perdew, Burke, and Ernzerhof was used for the exchange and correlation terms.[22] The atomic muffin-tin spheres used were 2.3 au for the Na atom, 1.7 au for the Ti atom, and 1.5 au for the O atom in $Na_2Ti_6O_{13}$, and 1.5 au for the Li atom, 1.9 au for the Ti atom, and 1.7 au for the O atom in $Li_2Ti_6O_{13}$. The plane-wave cutoff was $R_{MT} \times K_{max}$ = 7.0, where R_{MT} is the smallest atomic sphere radius in the unit cell and K_{max} is the magnitude of the largest k vector. Self-consistency was carried out on a 400 k-points mesh in the full Brillouin zone. The energy criterion for self-consistency was set to less than 0.001 eV per formula unit. The present structural parameters for $Na_2Ti_6O_{13}$ and $Li_2Ti_6O_{13}$ were used in the calculations. We also calculated the electronic structure of the hypothetical $Li_2Ti_6O_{13}$ structure in which the Li atoms occupied the original Na site.

Electrochemical Measurements. Electrochemical lithium insertion/extraction experiments for $Na_2Ti_6O_{13}$ and $Li_2Ti_6O_{13}$ were performed using lithium coin-type cells. The working electrode was prepared by mixing 62% active material, 31% acetylene black, and 7% polytetrafluoroethylene (PTFE) powder in weight by pressing the mixture onto an Al mesh having a diameter of 15 mm under a pressure of 20 MPa. The counter electrode was a Li foil having a diameter of 20 mm. The separator was a microporous polypropylene sheet. A solution of 1 M $LiPF_6$ in a 50:50 mixture of ethylene carbonate (EC) and diethylcarbonate (DEC) by volume (Kishida Chemical Co., Ltd.) was used as the electrolyte. Cells were constructed in an argon-filled glovebox, and electrochemical measurements were carried out with a constant current density per unit of mass of the active material, 10 mA g^{-1}, between 1.0 and 3.0 V at 25 °C after standing 6 h under an open circuit condition.

AC impedance measurements for $Na_2Ti_6O_{13}$ and $Li_2Ti_6O_{13}$ were conducted using a Solartron 1260 impedance analyzer operating at 10 mV applied ac amplitude at 13 MHz−10 Hz frequencies at room

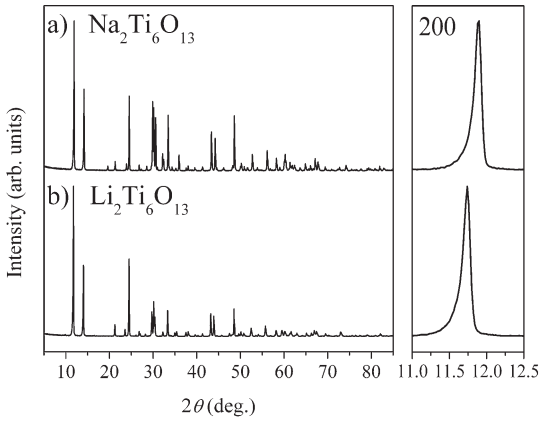

Figure 1. XRD patterns for (a) the precursor $Na_2Ti_6O_{13}$ and (b) the ion-exchanged $Li_2Ti_6O_{13}$ samples.

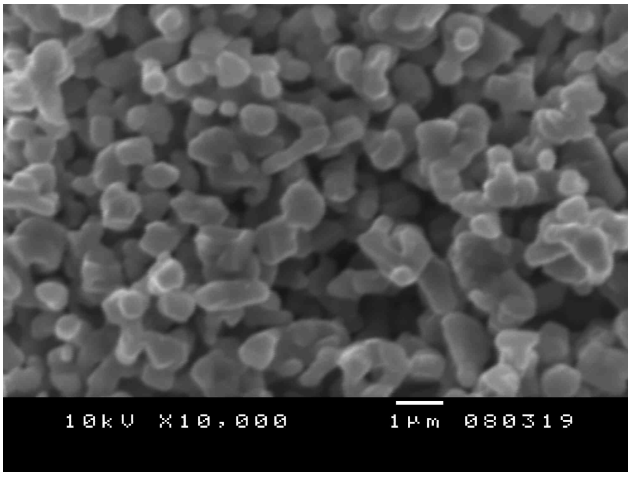

Figure 2. SEM photograph of the ion-exchanged $Li_2Ti_6O_{13}$ sample.

temperature in air. In the present study, the measurements were performed using the powder sample of 87.30 mg under the pressure of 1.5 MPa with the relative density of about 70%. The size of the measurement holder was 10 mm in diameter and 0.5 mm thickness.

RESULTS AND DISCUSSION

Ion-Exchange Synthesis of $Li_2Ti_6O_{13}$. The obtained precursor sample was identified to be a single phase of $Na_2Ti_6O_{13}$, monoclinic crystal system, and space group $C2/m$. No impurity phases were observed in the XRD pattern, as shown in Figure 1. The Na/Ti ratio was determined to be the stoichiometric composition of $Na_2Ti_6O_{13}$ by ICP-AES analysis. The lattice parameters of $Na_2Ti_6O_{13}$ were refined to be a = 15.0933(2) Å, b = 3.74300(2) Å, c = 9.1685(1) Å, and β = 99.017(1)° by the Rietveld method using the powder XRD data. The obtained lattice parameters were well consistent with those in previous reports.[10,11]

All of the $Li_2Ti_6O_{13}$ samples after ion-exchange experiments at various heating temperatures were also identified to be a single phase of the $Na_2Ti_6O_{13}$-related type structure, monoclinic crystal system, and space group $C2/m$. The SAED pattern also indicated that $Li_2Ti_6O_{13}$ belonged to the monoclinic system with an appropriate space group of Cm, $C2$, or $C2/m$. The ICP-AES

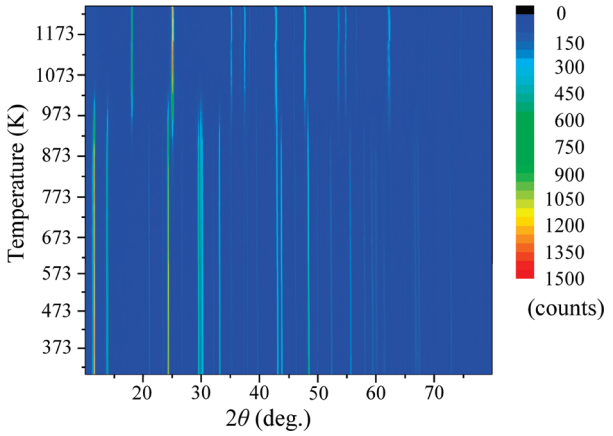

Figure 3. The continuous plot of high-temperature in situ XRD patterns of $Li_2Ti_6O_{13}$.

Table 1. Experimental and Crystallographic Data for $Na_2Ti_6O_{13}$ Using the Single-Crystal XRD Data

structural formula	$Na_2Ti_6O_{13}$
temperature (K)	295
crystal system	monoclinic
Laue group	$2/m$
space group	$C2/m$
lattice parameters	
a (Å)	15.110(1)
b (Å)	3.7440(5)
c (Å)	9.1693(15)
β (deg)	98.984(7)
crystal size (mm)	0.14 × 0.05 × 0.14
number of oscillation photos	120
oscillation angle (deg)	3
measured reflections	3555
independent reflections	1040
independent reflections (>3σ)	979
number of variables	65
R (%)	2.70
wR [$w = 1/\sigma^2F$] (%)	3.71

analysis confirmed that the residual Na-content gradually decreased with increasing soaking temperature from 290 to 380 °C. The chemical composition of the ion-exchange product at 290 °C was determined to be $Li_{1.87}Na_{0.13}Ti_6O_{13}$. The result indicated that the removal of Na was not complete at 290 °C. This fact was well consistent with a previous report.[9] On the other hand, the residual Na-content in the sample synthesized at 380 °C was less than 0.04 wt %, the value of which was within the experimental error of the analysis. Therefore, we used the sample synthesized at 380 °C for the following structural and electrochemical experiments of $Li_2Ti_6O_{13}$.

Figure 2 shows a typical SEM image of the $Li_2Ti_6O_{13}$ sample after ion-exchange experiment. The particle morphology and size remained nearly unchanged after ion-exchange reaction. The average particle size was about 1 μm. The FTIR absorption spectrum of the $Li_2Ti_6O_{13}$ sample confirmed that the present sample did not contain water species such as H_2O, OH^-, or H_3O^+ in the structure.

The XRD pattern of the ion-exchanged $Li_2Ti_6O_{13}$ sample is compared to that of the starting $Na_2Ti_6O_{13}$ sample (Figure 1). If the crystal structure of $Li_2Ti_6O_{13}$ is completely identical to that of $Na_2Ti_6O_{13}$, the 200 reflection peak around $2\theta = 12°$ would be shifted to higher angle together with a decrease in the *a*-axis length, because the ionic radius for Li^+ is much smaller than that for Na^+.[23] Contrary to this expectation, however, the 200 reflection peak in $Li_2Ti_6O_{13}$ shifted to lower angle, as shown in Figure 1. This fact means that sodium/lithium ion-exchange results in the expansion of the tunnel space. From this result, it can be speculated that the occupation site for the alkali ion may drastically change after ion-exchange, as previously reported in the layered $Li_2Ti_3O_7$.[8]

The phase stability and change of $Li_2Ti_6O_{13}$ upon heating were investigated by in situ XRD measurement. Figure 3 shows the continuous plot of the XRD patterns from 303 to 1243 K. Although $Li_2Ti_6O_{13}$ decomposes to the mixture of spinel-type $Li_4Ti_5O_{12}$ and rutile-type TiO_2 at around 973 K, it is clearly observed that this phase is stable below 873 K.

Crystal Structure of $Na_2Ti_6O_{13}$. The structure refinement of $Na_2Ti_6O_{13}$ was carried out using the single-crystal X-ray diffraction data with the reported atomic coordinates.[11] The converged final *R* and w*R* values and other experimental and crystallographic data are summarized in Table 1. Difference Fourier syntheses using the final atomic parameters showed no significant residual peaks. The final atomic coordinates and equivalent isotropic atomic displacement parameters are given in Table 2. The structure thus refined is basically the same as those in previous reports.[10,11] However, the present results provide a more precise structure of $Na_2Ti_6O_{13}$ including the atomic displacement parameters for all atoms.

Table 2. Atomic Coordinates and Equivalent Isotropic Displacement Parameters (Å^2) for $Na_2Ti_6O_{13}$ Determined Using the Single-Crystal XRD Data

atom	site	*x*	*y*	*z*	U_{eq} (Å^2)
Na1	4i	0.46112(8)	0	0.26583(18)	0.0367(5)
Ti1	4i	0.11444(2)	0	0.09726(4)	0.00475(11)
Ti2	4i	0.16630(2)	0	0.43635(4)	0.00429(12)
Ti3	4i	0.22804(2)	0	0.77086(4)	0.00421(11)
O1	2a	0	0	0	0.0131(7)
O2	4i	0.23996(10)	0	0.24471(18)	0.0059(4)
O3	4i	0.07049(10)	0	0.29239(17)	0.0073(4)
O4	4i	0.29701(10)	0	0.57131(16)	0.0058(4)
O5	4i	0.12659(10)	0	0.61413(17)	0.0079(4)
O6	4i	0.35669(10)	0	0.88297(17)	0.0066(4)
O7	4i	0.16371(10)	0	0.91319(17)	0.0106(5)

The crystal structure of $Na_2Ti_6O_{13}$ is shown in Figure 4. The basic framework structure of $Na_2Ti_6O_{13}$ consists of zigzag chains of triple edge-shared TiO_6 octahedra. All three TiO_6 octahedra were strongly distorted, and the individual Ti−O distance was in the wide range of 1.745(2)−2.243(2) Å. However, the bond valence sums for three Ti sites were 4.18 for the Ti1 site, 4.11 for the Ti2 site, and 4.19 for the Ti3 site. These values were well consistent with the formal valence of +4. From these facts, it can be concluded that the distortion for these TiO_6 octahedra is important to construct the $(Ti_6O_{13})^{2-}$ framework structure in $Na_2Ti_6O_{13}$.

The Na atom located in the rectangular tunnel space is surrounded by eight oxygen atoms in a distorted quadrangular prism at an average Na−O distance of 2.820 Å. As the Na atom slightly shifted to the center part of the tunnel, there are four shorter Na−O (average: 2.558 Å) and four longer Na−O distances (average: 3.082 Å). Accordingly, this coordination type is normal for the Na atom. It should be noted that the refined anisotropic atomic displacement parameter of U_{33} for the Na atom is 0.0662(10) Å^2. This value is much larger than those of U_{11} (0.0200(6) Å^2) and U_{22} (0.0247(6) Å^2), indicating an anisotropic characteristic parallel to the *c*-axis direction, as shown in Figure 4.

Crystal Structure of $Li_2Ti_6O_{13}$. The framework structure of $Li_2Ti_6O_{13}$ was first examined by ab initio structure determination method using the powder XRD data. The initial lattice parameters were determined to be $a = 15.347$ Å, $b = 3.753$ Å, $c = 9.149$ Å, and $\beta = 99.441°$ by an indexing procedure using the program N-TREOR[15] in EXPO2004.[16] The most probable space group was suggested to be $C2/m$. Next, the integrated intensities were extracted by the Le Bail method using the program Jana2006.[14] A profile function and background function of the Le Bail method used in the present study were pseudo-Voigt function and 20th-order Legendre function, respectively. An initial structure model was then obtained by the charge flipping (CF) method[17] using the extracted integrated intensities. Although the Li site could not be clearly determined by the CF method using the powder XRD data, the framework structure of $(Ti_6O_{13})^{2-}$ was successfully determined. In this stage, the lattice parameters of $Li_2Ti_6O_{13}$ were refined to be $a = 15.3244(2)$ Å, $b = 3.74847(2)$ Å, $c = 9.1429(1)$ Å, and $\beta = 99.419(1)°$ by the Rietveld method using the powder XRD data. The resultant reliability values, which were relatively large because of the preferred orientation of

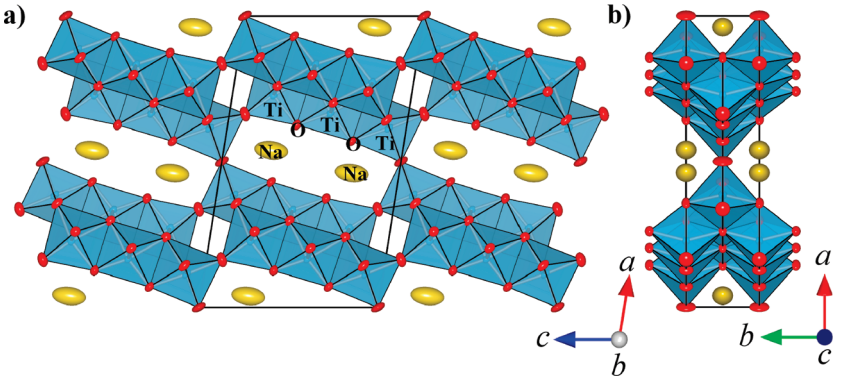

Figure 4. Crystal structure of $Na_2Ti_6O_{13}$ viewed along (a) the [010] and (b) the [001] directions. The solid box indicates the unit cell.

dx.doi.org/10.1021/cm103678e |*Chem. Mater.* 2011, 23, 2344–2352

the sample, were R_{wp} = 14.28% and R_p = 10.54% with a fit indicator of GOF = R_{wp}/R_e = 1.54. The obtained lattice parameters and the framework structure were well consistent with those in the previous report.[9,13]

Next, the crystal structure analysis of $Li_2Ti_6O_{13}$ using the powder ND data was initiated with the above-mentioned $(Ti_6O_{13})^{2-}$ framework structure (Figure 5a). The lithium site was determined using the difference Fourier synthesis map using the powder ND data. Figure 5b and c shows the difference Fourier synthesis maps of the y = 0 and y = 0.5 sections, respectively. The negative residual nuclear scattering length density can be clearly observed at the 4i position, suggesting the Li occupation. Therefore, the Li atom was introduced to the structure model in the following refinement. In the present refinement, the possibility of the residual sodium atoms in the structure could not be considered. Finally, the profile function parameters and all structure parameters of $Li_2Ti_6O_{13}$ were refined using the isotropic atomic displacement parameters. Difference Fourier syntheses using the final atomic parameters showed no significant residual peaks. Figure 6 shows the observed, calculated, and difference patterns for the Rietveld refinement of $Li_2Ti_6O_{13}$ using the powder ND data. The resultant reliability values were R_{wp} = 5.78% and R_p = 4.44% with a fit indicator of GOF = R_{wp}/R_e = 1.66. The lattice parameters for the $Li_2Ti_6O_{13}$ were refined by the Rietveld refinement using the powder ND data to be a = 15.3065(4) Å, b = 3.74739(8) Å, c = 9.1404(2) Å, and β = 99.379(2)°. The final atomic coordinates and isotropic atomic displacement parameters determined by Rietveld refinement using the powder ND data are listed in Table 3. The selected bond distances are shown in Table 4.

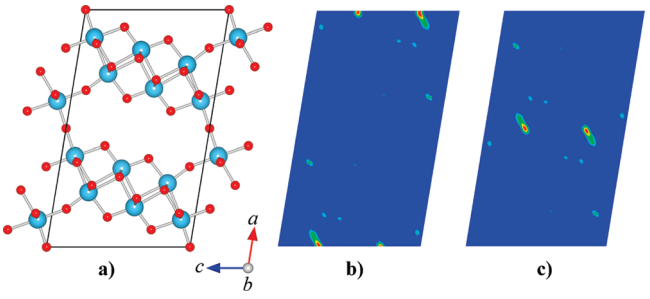

Figure 5. (a) The $(Ti_6O_{13})^{2-}$ framework in the $Li_2Ti_6O_{13}$ structure. The solid box indicates the unit cell. (b,c) The two-dimensional difference Fourier synthesis maps of $Li_2Ti_6O_{13}$ using the powder ND data of the y = 0 and y = 0.5 sections, respectively. The negative residual nuclear scattering length density destributions for the Li atoms are clearly observed in these maps.

Table 3. Atomic Coordinates and Equivalent Isotropic Displacement Parameters (Å^2) for $Li_2Ti_6O_{13}$ Determined Using the Powder ND Data

atom	site	x	y	z	U_{eq} (Å^2)
Li1	4i	0.450(1)	0.5	0.246(2)	0.026(4)
Ti1	4i	0.1150(2)	0	0.096(1)	0.006(2)
Ti2	4i	0.1677(5)	0	0.435(1)	0.006(2)
Ti3	4i	0.2309(3)	0	0.7720(9)	0.006(2)
O1	2a	0	0	0	0.005(1)
O2	4i	0.2380(3)	0	0.2423(6)	0.005(1)
O3	4i	0.0727(3)	0	0.2899(6)	0.005(1)
O4	4i	0.2963(3)	0	0.5734(6)	0.005(1)
O5	4i	0.1297(3)	0	0.6110(7)	0.005(1)
O6	4i	0.3549(3)	0	0.8885(6)	0.005(1)
O7	4i	0.1611(3)	0	0.9077(4)	0.005(1)

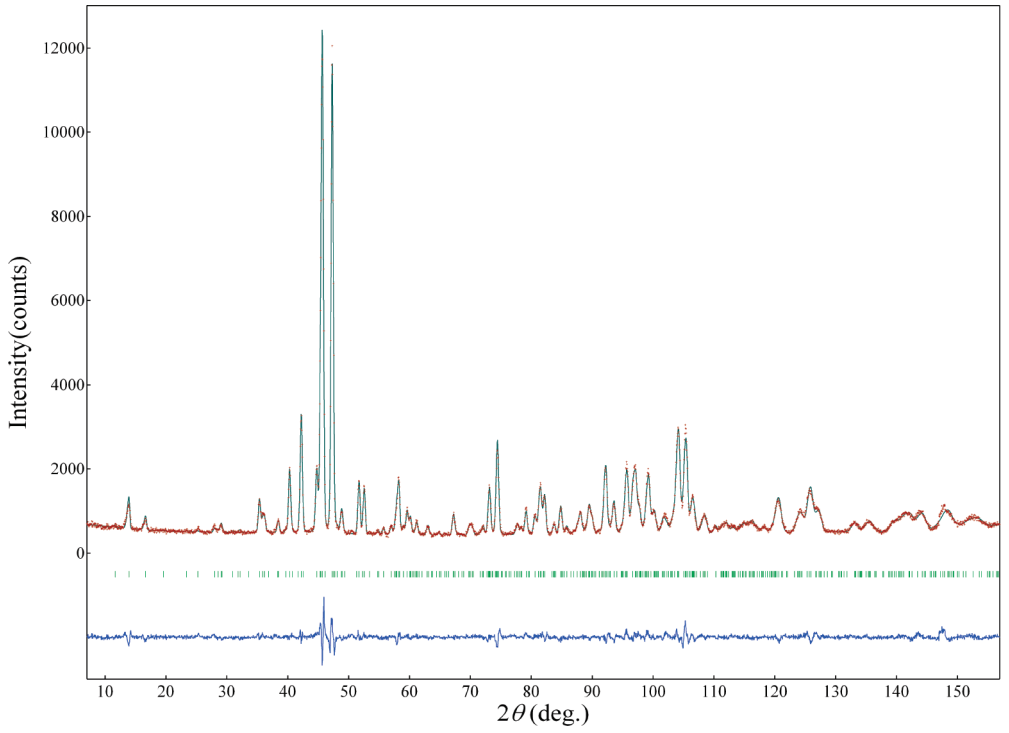

Figure 6. Observed, calculated, and difference pattern for the Rietveld refinement using the powder neutron diffraction data of $Li_2Ti_6O_{13}$. The short vertical lines below the profiles mark positions of all position Bragg reflections of $Li_2Ti_6O_{13}$.

dx.doi.org/10.1021/cm103678e |*Chem. Mater.* 2011, 23, 2344–2352

Table 4. Selected Bond Distances (Å) for $Li_2Ti_6O_{13}$

Li1−O1	2.50(2)	Li1−O3	1.84(2)
Li1−O5	1.94(2)	Li1−O7	2.03(2)
Ti1−O1	1.84(2)	Ti1−O2	2.12(1)
Ti1−O3	1.98(1)	Ti1−O6 × 2	1.93(1)
Ti1−O7	1.96(1)		
Ti2−O2	2.21(1)	Ti2−O3	1.80(1)
Ti2−O4 × 2	1.958(2)	Ti2−O4	2.16(1)
Ti2−O5	179(1)		
Ti3−O2 × 2	1.942(2)	Ti3−O4	2.21(1)
Ti3−O5	1.95(1)	Ti3−O6	2.02(1)
Ti3−O7	1.76(1)		

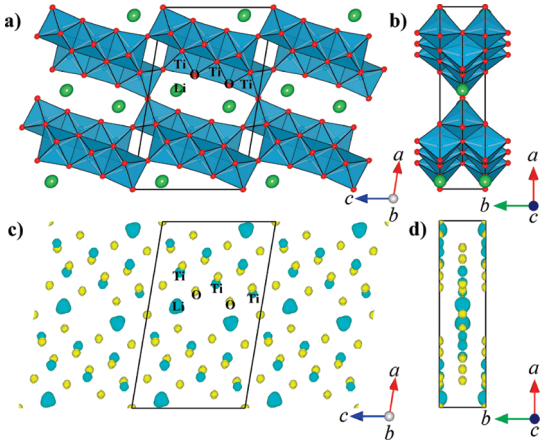

Figure 7. (a,b) Crystal structure of $Li_2Ti_6O_{13}$ viewed along the [010] and [001] directions. The solid box indicates the unit cell. (c,d) Three-dimensional nuclear scattering length density distribution with an iso surface level in 1.0 rm $Å^{-3}$ for $Li_2Ti_6O_{13}$ viewed along the [010] and [001] directions, respectively. The solid box indicates the unit cell. The distribution is colored with blue (gray) or yellow (white) to show a negative or positive nuclear scattering length, respectively.

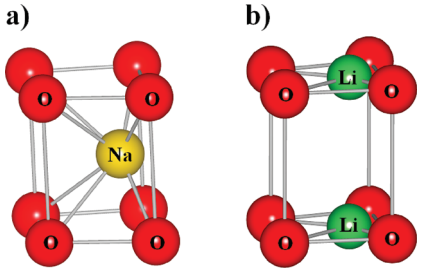

Figure 8. The oxygen coordination environments around (a) the Na atom in $Na_2Ti_6O_{13}$ and (b) the Li atom in $Li_2Ti_6O_{13}$.

The crystal structure and NSLDD of $Li_2Ti_6O_{13}$ are shown in Figure 7. The basic $(Ti_6O_{13})^{2-}$ framework in $Li_2Ti_6O_{13}$ is maintained nearly unchanged from that in the parent $Na_2Ti_6O_{13}$. All three TiO_6 octahedra were strongly distorted, and the Ti−O distances were in the wide range of 1.76(1)−2.21(1) Å. These features for the $(Ti_6O_{13})^{2-}$ unit were very similar to those observed in $Na_2Ti_6O_{13}$.

On the other hand, the most interesting feature of the $Li_2Ti_6O_{13}$ structure is the Li occupation site in the tunnel space.

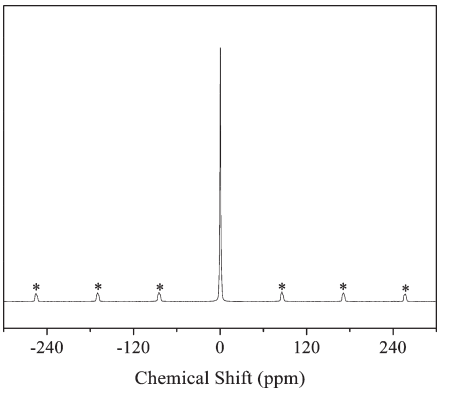

Figure 9. ^{7}Li-MAS NMR spectrum of $Li_2Ti_6O_{13}$ measured at room temperature. The marks "*" indicate spinning sidebands.

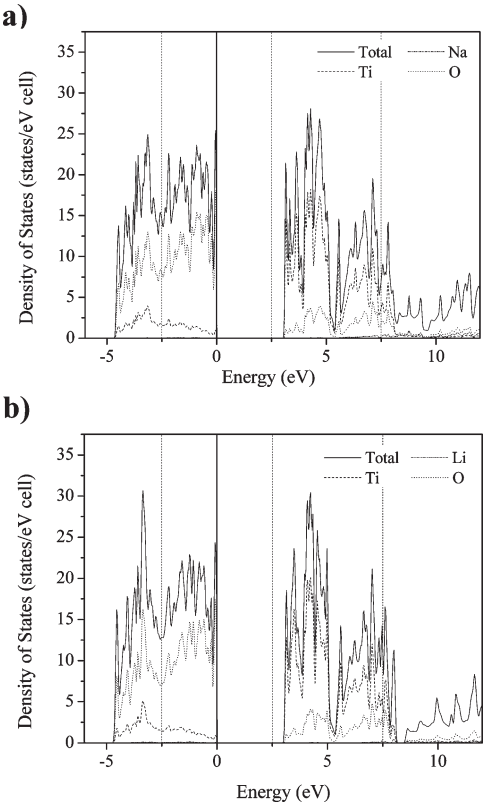

Figure 10. Calculated total and partial densities of states of (a) $Na_2Ti_6O_{13}$ and (b) $Li_2Ti_6O_{13}$.

In the parent $Na_2Ti_6O_{13}$ structure, the Na atom was surrounded by eight oxygen atoms (Figure 8a), as above-mentioned. This coordination type is normal for the Na atom. However, it seems unstable to be occupied by the Li atom to the similar oxygen coordination environment instead of Na. Although the Li atom often situated in the tetrahedral LiO_4 or octahedral LiO_6 site in many oxide compounds, such a coordination site could not be constructed in the present tunnel space of $Li_2Ti_6O_{13}$. We then examined the possible Li sites in accordance with the crystallographic constraint by the space group. Accordingly, we concluded that the Li atom had to shift to 1/2 along the *b* axis direction from the original Na site in the $Li_2Ti_6O_{13}$ structure

dx.doi.org/10.1021/cm103678e |*Chem. Mater.* 2011, 23, 2344–2352

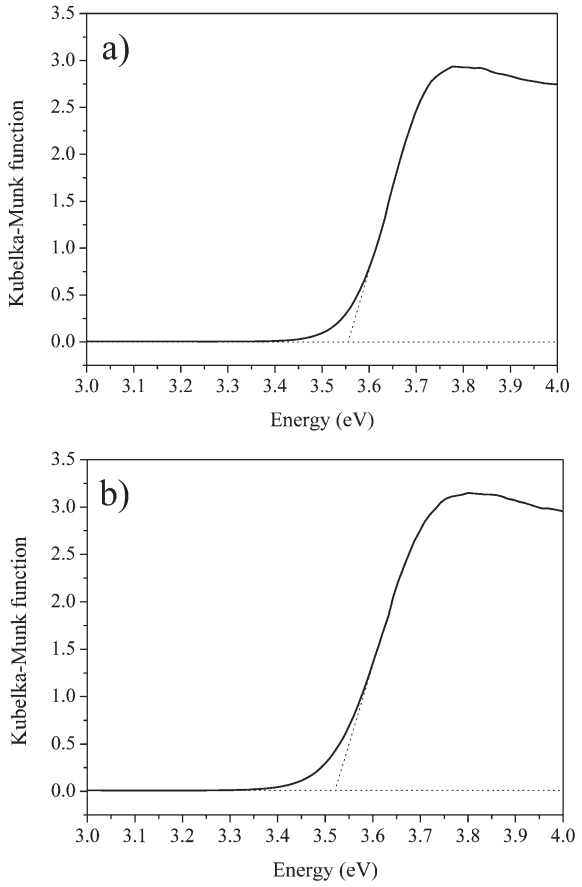

Figure 11. UV−vis absorption spectra of (a) $Na_2Ti_6O_{13}$ and (b) $Li_2Ti_6O_{13}$.

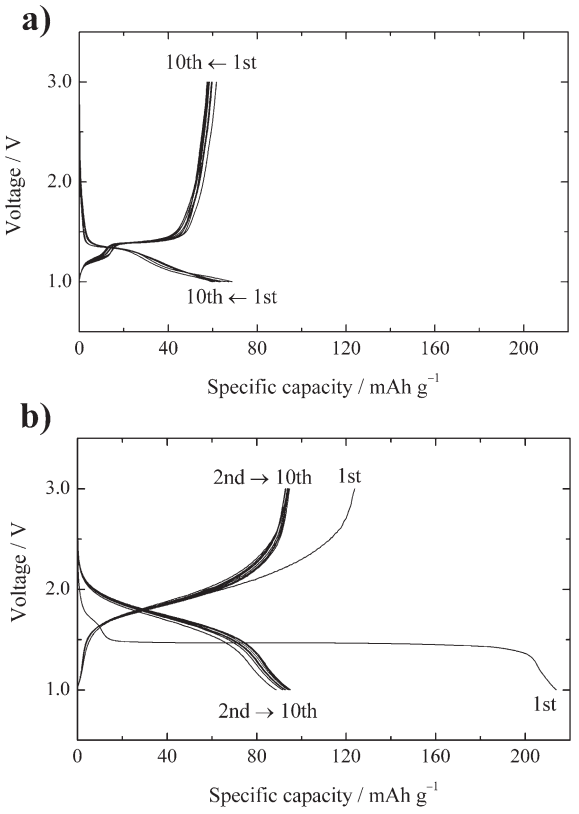

Figure 12. Charge−discharge properties of (a) $Na_2Ti_6O_{13}$ and (b) $Li_2Ti_6O_{13}$.

(Figure 8b). This feature was recently predicted;[13] however, the positional refinement was performed for the first time in the present study.

The resultant LiO_4 planar coordination was strongly distorted, and the four Li−O distances were 1.84(2), 1.94(2), 2.03(2), and 2.50(2) Å, suggesting planar (3 + 1) Li−O coordination. This coordination type is not normal for the Li atom in the literature. However, the calculated bond valence sum for the Li site was 1.015; the value is well consistent with the formal valence state of Li^+.

Figure 9 shows the ^{7}Li-MAS NMR spectrum of the $Li_2Ti_6O_{13}$ sample. As can be clearly observed, only one peak at 0.0 ppm appeared in the spectrum. This result may support the present Li occupation model that the Li atom situated at one crystallographic site.

It should be noted that the expansion of the tunnel space was confirmed by the present structure refinement. The oxygen−oxygen contact distance across the tunnel space was 3.366 Å for the O3−O5 distance in $Li_2Ti_6O_{13}$, which is much longer than the corresponding O3−O5 distance (3.225 Å) in $Na_2Ti_6O_{13}$. This fact can be explained by the positional shift from the original Na site in $Na_2Ti_6O_{13}$ to the new Li site in $Li_2Ti_6O_{13}$, as mentioned above.

Electronic Structures. The validity of the present structure model for $Li_2Ti_6O_{13}$ was elucidated from the total energy calculation by the FLAPW method in the present study. We calculated the electronic structures of two types of $Li_2Ti_6O_{13}$: one model was $Li_2Ti_6O_{13}$ determined in the present study, and the other model was hypothetical $Li_2Ti_6O_{13}$ structure in which the Li atoms occupied at the original Na site as in the parent $Na_2Ti_6O_{13}$ structure. The calculated total energies were −83 235.34 eV per formula unit for the present $Li_2Ti_6O_{13}$ structure and −83 234.37 eV per formula unit for the hypothetical structure. From this result, it is clear that the present $Li_2Ti_6O_{13}$ structure is more stable than that in the "$Na_2Ti_6O_{13}$"-type structure. Accordingly, it can be concluded that the planar LiO_4 coordination is more suitable in the tunnel space of $Li_2Ti_6O_{13}$ than is the original quadrangular "LiO_8" coordination.

Figure 10 shows the total and partial densities of states for $Na_2Ti_6O_{13}$ and $Li_2Ti_6O_{13}$. The origin of energy is at the Fermi level. The valence band of $Na_2Ti_6O_{13}$ in the range from −4.7 to 0.0 eV consists of the O-2p orbital hybridized with the Ti-3d orbital. The energy states ranging from 3.0 to 5.4 eV and 5.4 to 8.2 eV are attributed to the t_{2g} states and the e_g states of the Ti-3d orbital, respectively. Similarly to these results, the valence band of $Li_2Ti_6O_{13}$ in the range from −4.7 to 0.0 eV consists of the O-2p orbital hybridized with the Ti-3d orbital. The energy states ranging from 3.0 to 5.4 eV and 5.4 to 8.2 eV are attributed to the t_{2g} states and the e_g states of the Ti-3d orbital, respectively. The band gap values for $Na_2Ti_6O_{13}$ and $Li_2Ti_6O_{13}$ were estimated to be 3.0 eV. From these calculations, it is clearly understood that the Ti orbital and the O orbital decide the band gap. Accordingly, the band gap value for $Li_2Ti_6O_{13}$ is very similar to that in $Na_2Ti_6O_{13}$ because these compounds have the same framework structure of $(Ti_6O_{13})^{2-}$, as above-mentioned.

These features were experimentally confirmed by the UV−vis absorption spectra of $Na_2Ti_6O_{13}$ and $Li_2Ti_6O_{13}$ measured at room temperature, as shown in Figure 11. The estimated band gap for $Li_2Ti_6O_{13}$ is very similar to that for $Na_2Ti_6O_{13}$, the value of which is about 3.52 eV. This result is well consistent with the first-principles

dx.doi.org/10.1021/cm103678e |*Chem. Mater.* 2011, 23, 2344–2352

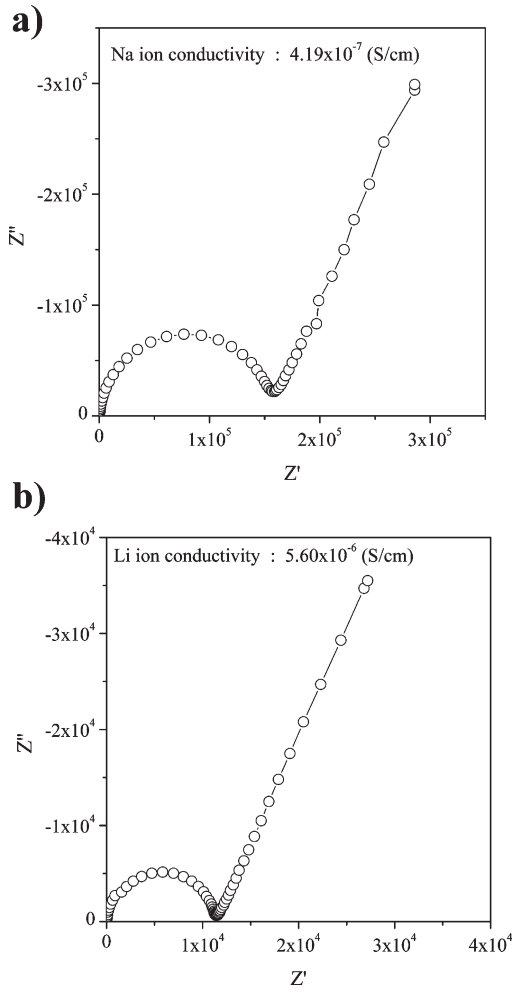

Figure 13. Nyquist plots of the ac impedance spectra of (a) $Na_2Ti_6O_{13}$ and (b) $Li_2Ti_6O_{13}$.

calculation. It should be noted that the calculated values are smaller than the experimental ones. This fact can be well explained as an underestimation of the calculation because the present study is based on the density-functional theory in its local approximation, which is strictly valid only for the ground state.

Electrochemical Properties. Figure 12a shows cycling performance of the electrochemical Li insertion−extraction reaction for the $Li_2Ti_6O_{13}$ sample in the voltage range between 1.0 and 3.0 V (vs Li/Li^+) at a current density of 10 mA g^{-1}. A flat potential plateau was observed at approximately 1.5 V (vs Li/Li^+) with the capacity of above 200 mAh g^{-1} for the first Li insertion reaction. However, the plateau disappeared with the following Li extraction reaction, and the profiles adopted a single sloping curve in the voltage range of 2.1−1.6 V. In addition, the Li insertion capacity drastically decreased from 210 to 90 mAh g^{-1} during the initial two cycles; however, a stable reversible capacity of approximately 90−95 mAh g^{-1} was observed during the following cycles. These results suggested that the first Li insertion reaction led to the degradation of the host $Li_2Ti_6O_{13}$ structure. On the other hand, a reversible Li insertion−extraction performance with a relatively small capacity of 60 mAh g^{-1} was observed at around 1.3 V in the case of $Na_2Ti_6O_{13}$, as shown in Figure 12b. These tendencies were basically similar to those reported for $Li_2Ti_6O_{13}$ and $Na_2Ti_6O_{13}$ recently.[13]

To examine the structural change in $Li_2Ti_6O_{13}$ and $Na_2Ti_6O_{13}$ before and after the electrochemical experiments, XRD measurements for the used electrodes were performed. The XRD pattern for the cycled $Li_2Ti_6O_{13}$ electrode showed the decrease in the peak intensity together with increasing peak width, suggesting the structural degradation for the $Li_2Ti_6O_{13}$ framework. On the contrary, the XRD pattern for the $Na_2Ti_6O_{13}$ electrode indicated that there was no damage to the framework structure, as previously demonstrated in the nanosized $Na_2Ti_6O_{13}$.[12] These facts may be affected by the difference in the structural stability of the Li inserted structure for $Na_2Ti_6O_{13}$ and $Li_2Ti_6O_{13}$.

Figure 13 shows ac impedance plots of the pressed powder samples for $Na_2Ti_6O_{13}$ and $Li_2Ti_6O_{13}$ at room temperature. The tail of impedance plots at a low-frequency side indicates the blocking of the electrodes for mobile Na ions or Li ions. The impedance plots at a high-frequency side show single semicircle behavior for both samples. The conductivity could not be separated into bulk and grain boundary in the present experiments. The total Na-ion conductivity in $Na_2Ti_6O_{13}$ was estimated to be $\sigma_{total} = 4.19 \times 10^{-7}$ S cm^{-1} at room temperature. On the other hand, the total Li-ion conductivity in $Li_2Ti_6O_{13}$ was $\sigma_{total} = 5.60 \times 10^{-6}$ S cm^{-1} at room temperature. This value is comparable to that in the ramsdellite-type $Li_2Ti_3O_7$, the value of which was reported to be $\sigma_{total} = 1.08 \times 10^{-6}$ S cm^{-1} at room temperature.[3] We are now trying to measure the conductivity of $Li_2Ti_6O_{13}$ at high temperatures.

CONCLUSIONS

In the present study, lithium titanate, $Li_2Ti_6O_{13}$, was successfully prepared from $Na_2Ti_6O_{13}$ as a parent compound via Na/Li ion-exchange in molten $LiNO_3$ at 380 °C. The phase purity and chemical composition of the ion-exchanged samples were well-characterized. The crystal structure of $Li_2Ti_6O_{13}$ was refined by Rietveld refinement using the powder neutron diffraction data. The basic $(Ti_6O_{13})^{2-}$ framework in $Li_2Ti_6O_{13}$ was maintained nearly unchanged from that in the parernt $Na_2Ti_6O_{13}$. The Li occupation site in the tunnel space shifted to the $y = 0.5$ position, and the moving resulted in the LiO_4 planar coordination in $Li_2Ti_6O_{13}$. The structural validity was confirmed by bond valence sums calculation, the data of ^{7}Li-MAS NMR and high-temperature in situ XRD measurements, and the results of the present first-principles calculation by the FLAPW method. This unusual Li−O coordination may affect the good lithium-ion conduction property even at room temperature among the lithium titanate compounds. On the other hand, the electrochemical Li insertion/extraction experiments revealed that the Li insertion reaction led to the degradation of the host $Li_2Ti_6O_{13}$ structure.

The low-temperature synthetic techniques such as ion-exchange reaction called "chimie douce" have resulted in major developments in the field of the solid-state chemistry of transition-metal oxides. In many cases, the framework structures of the parernt compounds were maintained nearly unchanged; however, the local structural changes around alkali atoms were recently revealed by the precise structural studies.[8] In the present study, an unusual LiO_4 planar coordination in $Li_2Ti_6O_{13}$ has been found for the first time by using Na/Li ion-exchange reaction.

ASSOCIATED CONTENT

Supporting Information. The observed, calculated, and difference patterns for the powder XRD Rietveld data of $Na_2Ti_6O_{13}$, the SAED pattern of $Li_2Ti_6O_{13}$, FTIR spectrum of

$Li_2Ti_6O_{13}$, the observed, calculated, and difference patterns for the powder XRD Rietveld data of $Li_2Ti_6O_{13}$ using the final structure model, and the XRD patterns of the cycled electrodes for $Na_2Ti_6O_{13}$ and $Li_2Ti_6O_{13}$ (PDF), and crystallographic information for $Na_2Ti_6O_{13}$ and $Li_2Ti_6O_{13}$ (CIF). This material is available free of charge via the Internet at http://pubs.acs.org.

AUTHOR INFORMATION

Corresponding Author

*E-mail: kataoka-kunimitsu@aist.go.jp (K.K.); j.akimoto@aist.go.jp (J.A.).

ACKNOWLEDGMENT

We thank Dr. Y. Sakiyama of Toray Research Center, Inc., for her experimental help and discussions regarding the ^{7}Li-MAS NMR measurement.

REFERENCES

(1) Colbow, K. M.; Dahn, J. R.; Haering, R. R. *J. Power Sources* **1989**, *26*, 397–402.
(2) Ohzuku, T.; Ueda, A.; Yamamoto, J. *J. Electrochem. Soc.* **1995**, *142*, 1431–1435.
(3) Boyce, J. B.; Mikkelsen, J. C., Jr. *Solid State Commun.* **1979**, *31*, 741–745.
(4) Gover, R. K. B.; Tolchard, J. R.; Tukamoto, H.; Murai, T.; Irvine, J. T. S. *J. Electrochem. Soc.* **1999**, *146*, 4348–4353.
(5) Arroyo de Dompablo, M. E.; Moran, E.; Varez, A.; Garcia-Alvarado, F. *Mater. Res. Bull.* **1997**, *32*, 1221–1227.
(6) Chan, F.; Li, R.; Hou, M.; Liu, L.; Wang, R.; Deng, Z. *Electrochim. Acta* **2005**, *51*, 61–65.
(7) Kikkawa, S.; Yasuda, F.; Koizumi, M. *Mater. Res. Bull.* **1985**, *20*, 1221–1227.
(8) Chiba, K.; Kijima, N.; Takahashi, Y.; Idemoto, Y.; Akimoto, J. *Solid State Ionics* **2008**, *178*, 1725–1730.
(9) England, W. A.; Goodenough, J. B.; Wiseman, P. J. *J. Solid State Chem.* **1983**, *49*, 289–299.
(10) Torres-Martínez, L. M.; Juárez-Ramírez, I.; Ángel-Sánchez, K. D.; Garza-Tovar, L.; Cruz-López, A.; Ángel, G. D. *J. Sol.-Gel Sci. Technol.* **2008**, *47*, 158–164.
(11) Andersson, S.; Wadsley, A. D. *Acta Crystallogr.* **1962**, *15*, 194–201.
(12) Dominko, R.; Baudrin, E.; Umek, P.; Arčon, D.; Gaberšček, M.; Jamnik, J. *Electrochem. Commun.* **2006**, *8*, 673–677.
(13) Pérez-Flores, J. C.; Kuhn, A.; Gracia-Alvarado, F. *J. Power Sources* **2011**, *196*, 1378–1385.
(14) Petříček, V.; Dušek, M.; Palatinus, L. *Jana2006. The crystallographic computing system*; Institute of Physics: Praha, Czech Republic, 2006.
(15) Altomare, A.; Giacovazzo, C.; Guagliardi, A.; Moliterni, A. G. G.; Rizzi, R.; Werner, P.-E. *J. Appl. Crystallogr.* **2000**, *33*, 1180–1186.
(16) Altomare, A.; Burla, M. C.; Camalli, M.; Carrozzini, B.; Cascarano, G. L.; Giacovazzo, C.; Guagliardi, A.; Moliterni, A. G. G.; Polidori, G.; Rizzi, R. *J. Appl. Crystallogr.* **1999**, *32*, 339–340.
(17) Palatinus, L.; Chapuis, G. *J. Appl. Crystallogr.* **2007**, *40*, 786–790.
(18) Ohoyama, K.; Kanouchi, T.; Nemoto, K.; Ohashi, M.; Kajitani, T.; Yamaguchi, Y. *Jpn. J. Appl. Phys.* **1998**, *37*, 3319–3326.
(19) Izumi, F.; Dilania, R. A. *Recent Research Developments in Physics*, 3, II; Transworld Research Network: Trivandrum, 2002; pp 699−726.
(20) Momma, K.; Izumi, F. *J. Appl. Crystallogr.* **2008**, *41*, 653–658.
(21) Blaha, P.; Schwarz, K.; Madsen, G.; Kvasnicka, D.; Luitz, J. *WIEN2k, Augmented Plane Wave + Local Orbitals Program for Calculating Crystal Properties*; Technische Universität Wien: Vienna, 2001.
(22) Perdew, P.; Burke, K.; Ernzerhof, M. *Phys. Rev. Lett.* **1996**, *77*, 3865–3868.
(23) Shanon, R. D. *Acta Crystallogr.* **1976**, *A32*, 751–767.